JOURNAL OF AIRCRAFT
Vol. 36, No. 6, November–December 1999

Estimating Aerodynamic Characteristics of Automatic Landing Flight Experiment Vehicle Using Flight Data

Masaaki Yanagihara* and Masashi Shigemi†
National Aerospace Laboratory, Tokyo 181-0015, Japan
and
Takanobu Suito‡
National Space Development Agency, Tokyo 105-8060, Japan

The Automatic Landing Flight Experiment (ALFLEX) project was conducted as part of the research on the H-II orbiting plane-experimental (HOPE-X) unmanned reentry vehicle. One of the aims of the ALFLEX was to estimate the low-speed aerodynamic characteristics of a delta-winged vehicle with wingtip fins and experiments for this purpose, such as α/β sweep and control surface excitation, were conducted during hanging (suspended from a mother ship) and automatic landing test flights. When flight test data are analyzed, the aerodynamic characteristics of the ALFLEX vehicle are estimated and the results are compared with those predicted by wind-tunnel tests. Flight results show that estimated characteristics are similar to the predictions except for a few characteristics. Although the results from the hanging flight tests exhibit scattering that is due to measurement errors caused by the effects of an umbilical cable, the hanging test method will be useful if this problem is solved by means such as using an internal battery to supply power to the vehicle instead of the umbilical cable.

Nomenclature

C_D	= drag coefficient
C_L	= lift coefficient
$C_{L_0}, C_{L_\alpha}, \ldots$	= aerodynamic model parameters
C_l	= rolling moment coefficient
C_m	= pitching moment coefficient
C_n	= yawing moment coefficient
C_Y	= side-force coefficient
H	= altitude
P	= roll rate
Q	= pitch rate
R	= yaw rate
t	= time
x	= x coordinate value in runway axis system
α	= angle of attack
β	= sideslip angle
γ	= flight-path angle
δa	= aileron angle, $(\delta_{eR} - \delta_{eL})/2$
δe	= elevator angle, $(\delta_{eR} + \delta_{eL})/2$, where δ_{eL} and δ_{eR} are left and right elevon angles, respectively
δ_r	= rudder angle, $(\delta_{rR} + \delta_{rL})/2$, where δ_{rL} and δ_{rR} are left and right rudder angles, respectively
δ_s	= speed-brake angle, $(\delta_{SR} + \delta_{SL})/2$, where δ_{SL} and δ_{SR} are left and right speed-brake angles, respectively
Θ	= pitch attitude angle
σ	= standard deviation
Φ	= roll attitude angle

Subscript

trim	= trimmed value

Superscript

ˆ	= nondimensional value

Introduction

THE National Aerospace Laboratory (NAL) and the National Space Development Agency of Japan (NASDA) have been conducting joint research on the H-II orbiting plane-experimental (HOPE-X) vehicle, an unmanned experimental vehicle that is to be launched by an H-II A rocket to establish key technologies for reusable space transportation systems.[1] The Automatic Landing Flight Experiment (ALFLEX) program was conducted as part of this research with a 37% dynamically scaled model of the planned HOPE-X designed to have aerodynamic and inertial characteristics equivalent to those of the full-scale vehicle. The aims of the ALFLEX program were 1) to evaluate the low-speed aerodynamic characteristics of a delta-winged vehicle with wingtip fins, 2) to develop and verify automatic landing (AL) technologies, and 3) to evaluate a flight test methodology by using a scaled model. For those purposes, hanging (suspended) and AL flight tests were conducted at Woomera in Australia from May to August, 1996, and a total of 13 landing trials were successfully carried out. The sequence of the experiment and a schematic of the vehicle are shown in Figs. 1 and 2, respectively. In this paper, the aerodynamic characteristics of the ALFLEX vehicle estimated from flight test data are presented and compared with those predicted from the wind-tunnel test database used for designing the flight-control system.

Aerodynamic Characteristics Estimation by Flight Test

During the ALFLEX program, both hanging and AL test flights were conducted.

The hanging flight (HF) test involves the suspension of the vehicle by a hanging wire through gimbals with two axes set at the designed center-of-gravity (CG) point. The vehicle is flown with a freedom of rotation around the pitch, roll, and yaw axes.[2] The HF configuration is shown in Fig. 3. The vehicle's flight-control system and aerodynamic characteristics were evaluated by HF tests before the AL flights.

In the AL flight tests, the vehicle is released at the altitude of 1500 m and goes into a steep descent at a flight path of −30 deg under the navigation, guidance, and control of the onboard computer. It

Presented as Paper 97-3485 at the AIAA Atmospheric Flight Mechanics Conference, New Orleans, LA, 11–13 August 1997; received 5 November 1998; revision received 20 March 1999; accepted for publication 3 April 1999.

*Head, Airworthiness Laboratory, Flight Division, 6-13-1 Osawa, Mitaka. Member AIAA.
†Head, Aircraft Aerodynamics Laboratory, Aerodynamics Division.
‡Engineer, Winged Space Vehicle Office, 2-4-1 Hamamatsucho, Minato.

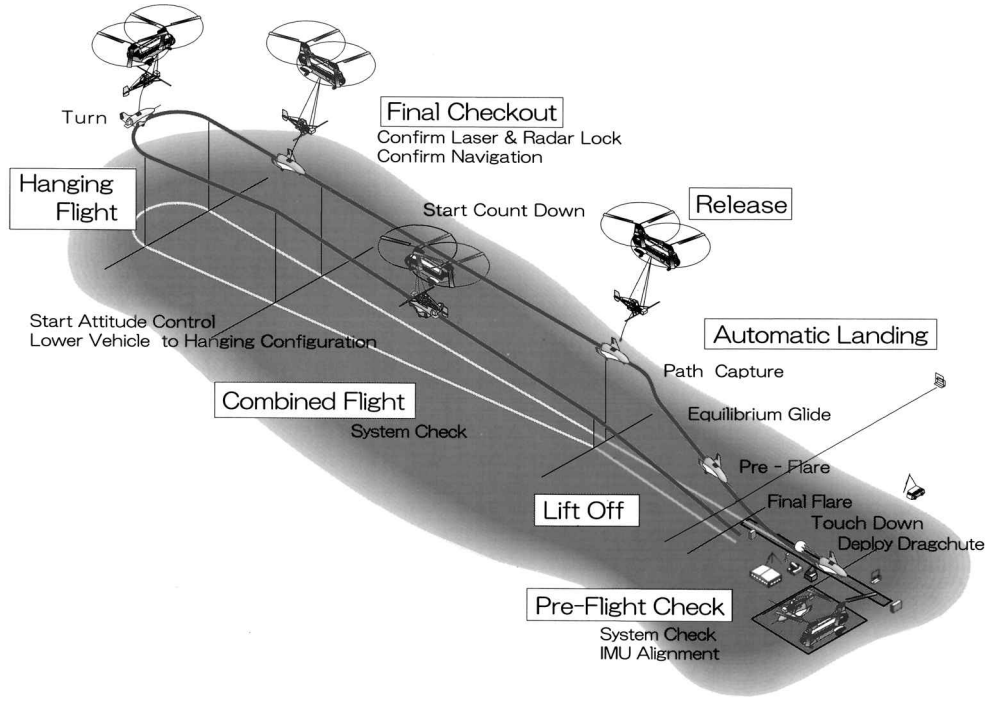

Fig. 1 ALFLEX mission profile. IMU, inertial measurement unit.

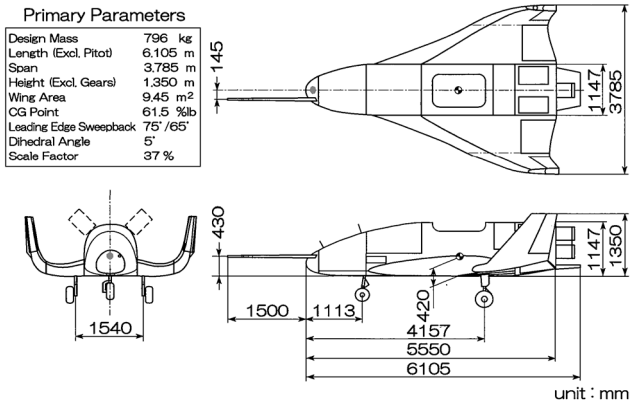

Fig. 2 ALFLEX three-view drawing. CG, center of gravity.

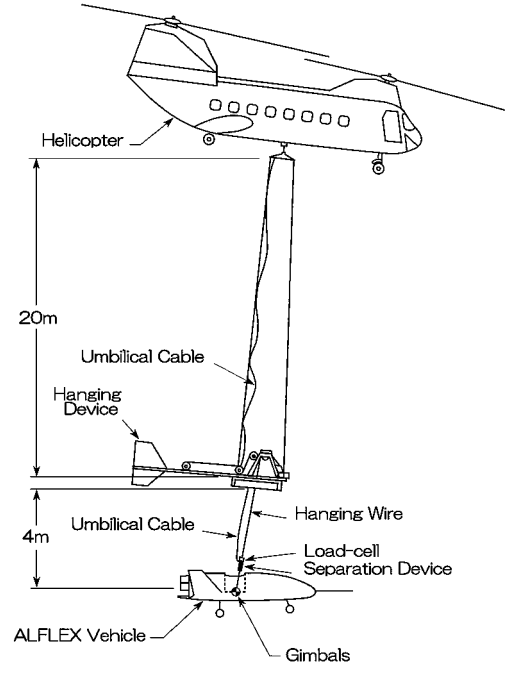

Fig. 3 Five-degree-of-freedom HF.

glides with aerodynamic control surfaces, such as elevons, rudders and speed brakes, and lands on the runway. Figure 4 shows the nominal flight profile of the AL flights.

To estimate the aerodynamic characteristics of the vehicle, dynamic and quasi-steady maneuvers were performed.

Dynamic flight tests are conducted to identify an aerodynamic model, including dynamic effects. Control surface excitation tests, in which the elevator, aileron, or rudder is deflected according to an M-sequence signal (a pseudorandom square-wave signal), and α, β, or Φ command step input tests were performed. An aerodynamic model that has a certain analytic model structure was then fit to the resulting test data by a least-squares method to obtain estimates of model parameters. Figure 5 shows an example of the elevator excitation test conducted in the HF. The dashed line indicates the M-sequence elevator deflection command signal. Although the elevator behaves as if a pulse signal is input because the flight control system produces an inverse command signal to stabilize the motion, the vehicle performs a pitching maneuver in response to elevator input. As the dynamic flight tests in the HFs, two trials of the elevator excitation test, three trials of the α command step input test, one trial each of the aileron and the rudder excitation tests, three trials of the β command step input test, and two trials of the Φ command step input test were conducted. Aerodynamic model identification was performed with all of the resulting data. In AL flights, the vehicle flew at a trimmed condition during the equilibrium glide phase for 15–20 s before the preflare was initiated. With ~10 s during this equilibrium phase, the control surface excitation tests were performed. Figure 6 shows an example of the elevator excitation test. The vehicle performs a pitching maneuver in response to elevator input, but the flight path is affected by the maneuver only slightly. Eight out of the 13 AL flights included control surface excitation tests that consisted of four trials of elevator excitation for longitudinal aerodynamic model identification and two trials each of aileron and rudder excitation for lateral-directional model identification.

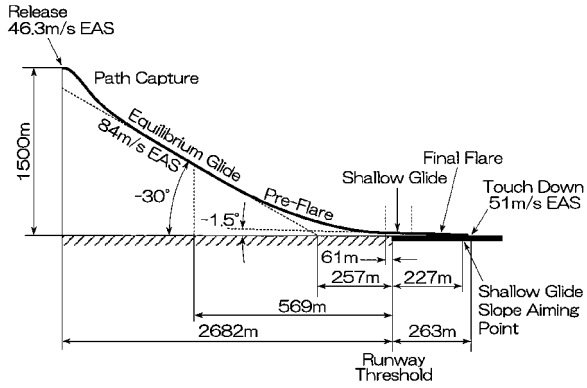

Fig. 4 ALFLEX nominal flight path. EAS, equivalent air speed.

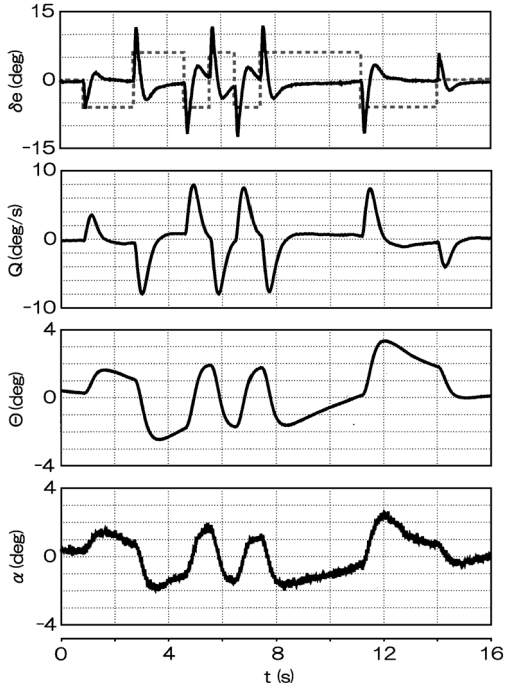

Fig. 5 Elevator excitation test (HF).

Quasi-steady flight tests were needed to investigate the trimmed flight characteristics of the vehicle. For this purpose, α and β sweep tests were carried out. In the sweep tests, the attitude of the vehicle is altered quasi statically by changing the α or β command to the control system gradually. As the rate is kept small, the vehicle maintains a trimmed flight condition while changing the attitude. The aerodynamic coefficients and the angles of the control surfaces during the maneuver show the trimmed flight characteristics. Figure 7 shows time histories of an α sweep test conducted in the HF. In this trial, the angle of attack command was altered between -5 and $+5$ deg at a rate of 0.5 deg/s. In the HFs, three trials each of α and β sweep tests were carried out. Although a dynamic flight test could be conducted in the AL flight tests with the equilibrium glide phase, a quasi-steady flight could not be performed during the AL flight, which lasts only some 40 s and requires a precise landing. As a result, the equilibrium glide data obtained from the five flights in which control surface excitation tests were not performed were used to evaluate trimmed flight characteristics.

The dynamic and the quasi-steady test methods each have advantages and disadvantages. If the aerodynamic model structure is not appropriate, the dynamic flight test identification may yield unreliable results. On the other hand, only the trimmed flight characteristics are derived from the quasi-steady flight tests. The dynamic effects and the control surface effectiveness cannot be measured

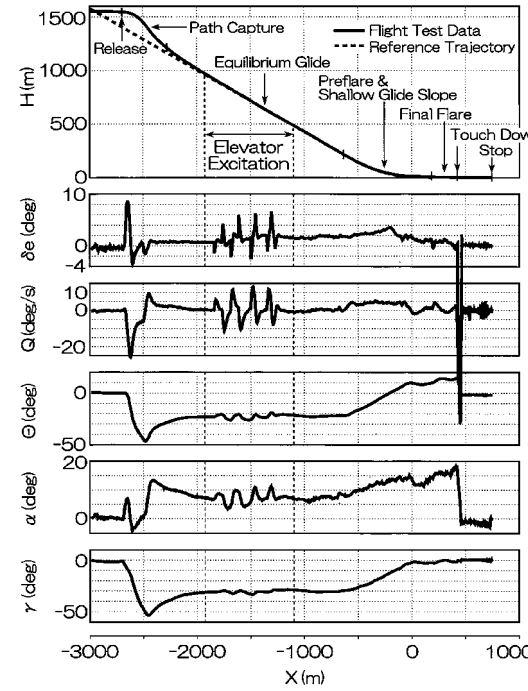

Fig. 6 Elevator excitation test (AL flight).

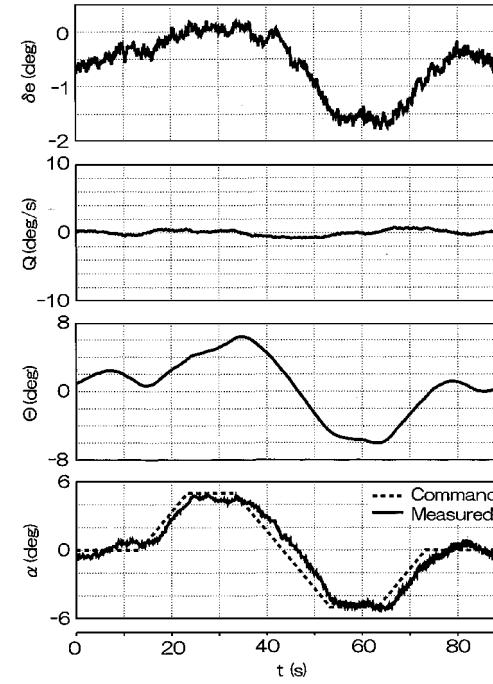

Fig. 7 α sweep test (HF).

from the quasi-steady maneuvers. The test methods were therefore used in combination. The trimmed characteristics were calculated with the identified model, and they were compared with the results of the quasi-steady tests. The suitability of the model structure was evaluated by analysis of the degree of coincidence between these two results.

Results of Estimation of Longitudinal Aerodynamic Characteristics

Table 1 shows the analytic model structures used for longitudinal aerodynamic model identification from dynamic flight-test data and the estimated parameters. For brevity, the model estimated from HF tests will be referred to hereinafter as the HF-identified model, and

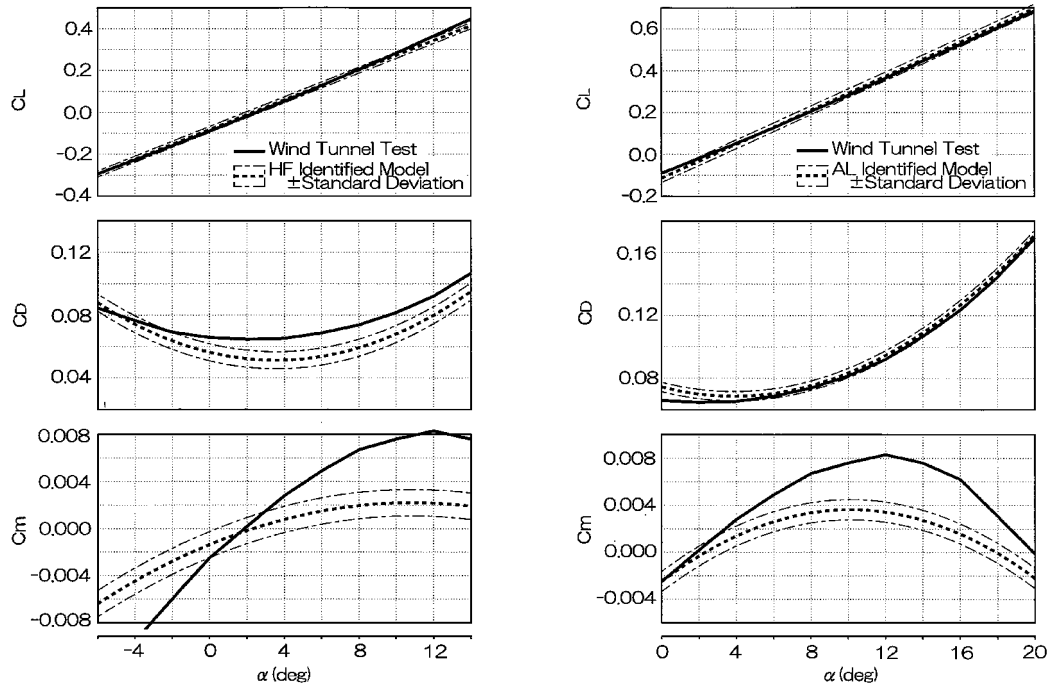

a) Hanging flight **b) Automatic landing flight**

Fig. 8 Longitudinal identified model.

that estimated from AL tests will be referred to as the AL-identified model. The tables also show the predicted parameters obtained when the same model structures are fit to a functional aerodynamic model gained based on the wind-tunnel test. This functional model is hereinafter referred to as the wind-tunnel model. A model structure for the lift coefficient is linear, but those for the drag and the pitching moment coefficients are quadratic forms to reflect the nonlinearity with angle of attack. The reason why the longitudinal model structures for the AL flights are expanded at $\alpha = 8$ deg is because the vehicle flies at approximately this value of the angle of attack during the equilibrium glide phase. A pitch damping term (C_{m_q}) is included in the pitching moment model to represent the dynamic effect. The angle of attack varied between -6 and 14 deg in the HF tests and between 4 and 11 deg in the AL flight tests. The range in the AL flight is smaller than that of the HF because the α step input tests could not be performed as they were in the HF tests. To compensate for this, the flight data during the path capture phase are also used for longitudinal model identification and the total variation range of the angle of attack is between 0 and 20 deg. The values inside parentheses in a row of predicted parameters are the uncertainties of the wind-tunnel database (variation). These were estimated by examination of the errors between wind-tunnel data and flight test results of another winged reentry vehicle, the U.S. Space Shuttle. The absence of the variation value indicates that the uncertainties are not defined. The values in parentheses in a row of estimated parameters are the 3σ values (three times the standard deviation) of the least-squares estimate of each parameter. The italics indicate the parameters for which the difference between the prediction and the estimate is larger then the variation. Judging from Table 1, although a difference between the estimated and the predicted values for the effect of the elevator ($C_{L_{\delta e}}$) is a little out of the variation, the differences for other parameters of the lift coefficient and the pitching moment coefficient models are within the variations in both the HF- and AL-identified models. The pitch damping parameters (C_{m_q}) of the identified models are 118% (HF) or 97% (AL) of the predicted values. The estimated values of the elevator effect ($C_{m_{\delta e}}$) are 81% (HF) or 91% (AL) of the predicted values. The drag coefficient of the AL-identified model is fairly close to that of the predicted model, and the identified value of the speed-brake effect ($C_{D_{\delta s}}$) is 96% of the predicted value. There is a large difference, however, between the estimated and the predicted values of the constant term in the drag coefficient model (C_{D_0}) in the HF-identified model.

Figure 8 shows the relation between the HF- or the AL-identified model and the wind-tunnel model, with α as the abscissa parameter. In these figures, the dashed curves indicate the identified models, the solid curves indicate the wind-tunnel model, and the dashed–dotted curves indicate the standard deviation (σ) of the flight test data around the identified models. The HF-identified model and the wind-tunnel model show good agreement for the lift coefficient. For the drag coefficient, there are differences for not only the constant term but for α^2 and α terms. For the pitching moment coefficient, there seems to be a fairly large difference although all the estimated parameters are within the variations. For the AL-identified model, the lift and the drag coefficient models are very close to those of the wind-tunnel model, and the scattering of the flight test data used for the drag coefficient identification, as indicated by the width of the area between the dashed–dotted curves, is much smaller than that in the HF-identified model. The pitching moment coefficient shows almost the same characteristics as those of the HF-identified model, indicating that there is a difference between the identified and the wind-tunnel pitching moment models.

Figure 9 shows the longitudinal trimmed characteristics obtained by analysis of the quasi-steady flight test data (α sweep and the equilibrium glide). In these figures, the aerodynamic coefficients and the angles of control surfaces at the trimmed flight condition calculated from the quasi-steady flights are indicated by dots ($\cdot$), with α as the abscissa parameter, and the trimmed characteristics calculated with the wind-tunnel model or the HF/AL- identified model are also shown for reference with solid curves or dashed curves, respectively. Judging from these figures, the results of the quasi-steady flights coincide with the results calculated with the identified models except for the drag coefficient of the HF. It can be seen that the results for the trimmed drag coefficient ($C_{D_{\text{trim}}}$) extracted from the α sweep tests in the HFs separate into two groups with a bias of $\sim$0.02. In this graph the results of two α sweep test trials ($\alpha = -5 \Leftrightarrow +5$ deg and $\alpha = 0 \Rightarrow 12$ deg) are indicated. The difference between these two groups for lift and pitching moment characteristics is not so large, and there is not such a large discrepancy in the drag results extracted from the AL flights. As the reason for this difference seems to be some measurement error, a sensitivity analysis was carried out to identify the error source. Because the aerodynamic force acting on

Table 1 Longitudinal aerodynamic model

		Aerodynamic model parameters														
Flight	Parameter	C_{L_0}	C_{L_α}	$C_{L_{\delta e}}$	$C_{L_{\delta s}}$	C_{D_0}	$C_{D_{\alpha 2}}$	C_{D_α}	$C_{D_{\delta e}}$	$C_{D_{\delta s}}$	C_{m_0}	$C_{m_{\alpha 2}}$	C_{m_α}	C_{m_q}	$C_{m_{\delta e}}$	$C_{m_{\delta s}}$
HF[a]	Prediction	−0.086	2.093	*0.697*	−0.057	*0.068*	0.997	−0.083	0.036	0.060	−0.002	−0.181	0.089	−0.761	−0.233	0.017
	(Variation)	(±0.022)	(±0.401)	(±0.180)	——	(±0.007)	——	——	——	——	(±0.010)	——	(±0.121)	——	(±0.060)	——
	HF identification	−0.082	2.028	*0.515*	——	*0.056*	1.318	−0.164	−0.031	——	−0.001	−0.099	0.038	−0.895	−0.189	——
	(3σ)	(0.001)	(0.008)	(0.018)	——	(0.000)	(0.031)	(0.006)	(0.007)	——	(0.000)	(0.006)	(0.001)	(0.032)	(0.001)	——
AL[b]	Prediction	0.208	2.206	*0.723*	−0.074	0.075	1.157	0.200	0.105	0.054	0.008	−0.277	0.034	−0.794	−0.244	0.017
	(Variation)	(±0.022)	(±0.401)	(±0.180)	——	(±0.007)	——	——	——	——	(±0.010)	——	(±0.121)	——	(±0.060)	——
	AL identification	0.211	2.320	*0.411*	−0.020	0.075	1.292	0.186	−0.025	0.052	0.003	−0.196	0.015	−0.768	−0.224	0.011
	(3σ)	(0.002)	(0.012)	(0.032)	(0.004)	(0.000)	(0.014)	(0.004)	(0.005)	(0.001)	(0.000)	(0.003)	(0.001)	(0.028)	(0.002)	(0.000)

[a]Aerodynamic model structure: $C_L = C_{L_0} + (C_{L_\alpha})\alpha + (C_{L_{\delta e}})\delta e + (C_{L_{\delta s}})\delta s$, $C_D = C_{D_0} + (C_{D_{\alpha 2}})\alpha^2 + (C_{D_\alpha})\alpha + (C_{D_{\delta e}})\delta e + (C_{D_{\delta s}})\delta s$, $C_m = C_{m_0} + (C_{m_{\alpha 2}})\alpha^2 + (C_{m_\alpha})\alpha + (C_{m_q})\hat{q} + (C_{m_{\delta e}})\delta e + (C_{m_{\delta s}})\delta s$.

[b]Aerodynamic model structure ($\alpha_0 = 8$ deg): $C_L = C_{L_0} + C_{L_\alpha}(\alpha - \alpha_0) + (C_{L_{\delta e}})\delta e + (C_{L_{\delta s}})\delta s$, $C_D = C_{D_0} + C_{D_{\alpha 2}}(\alpha - \alpha_0)^2 + C_{D_\alpha}(\alpha - \alpha_0) + (C_{D_{\delta e}})\delta e + (C_{D_{\delta s}})\delta s$, $C_m = C_{m_0} + C_{m_{\alpha 2}}(\alpha - \alpha_0)^2 + C_{m_\alpha}(\alpha - \alpha_0) + (C_{m_q})\hat{q} + (C_{m_{\delta e}})\delta e + (C_{m_{\delta s}})\delta s$.

Table 2 Lateral-directional aerodynamic model[a]

		Aerodynamic model parameters														
Flight	Parameter	C_{Y_0}	C_{Y_β}	$C_{Y_{\delta a}}$	$C_{Y_{\delta r}}$	C_{l_0}	C_{l_β}	C_{l_p}	C_{l_r}	$C_{l_{\delta a}}$	$C_{l_{\delta r}}$	C_{n_0}	C_{n_β}	C_{n_p}	C_{n_r}	$C_{n_{\delta a}}$	$C_{n_{\delta r}}$
HF ($\alpha = 0$ deg)	Prediction	*0.001*	*−0.661*	*−0.052*	0.205	−0.000	−0.055	−0.248	−0.030	−0.144	0.073	−0.001	−0.019	0.163	−0.455	0.024	−0.110
	(Variation)	(±0.006)	(±0.111)	(±0.010)	(±0.063)	(±0.004)	(±0.034)	——	——	(±0.022)	(±0.017)	(±0.001)	(±0.023)	——	——	(±0.014)	(±0.024)
	HF identification	*0.013*	*−0.795*	*−0.184*	0.155	0.001	−0.039	−0.186	[−0.030]	−0.123	0.061	−0.001	0.002	[0.163]	−0.335	0.025	−0.095
	(3σ)	(0.000)	(0.007)	(0.018)	(0.013)	(0.000)	(0.000)	(0.011)	——	(0.001)	(0.001)	(0.000)	(0.001)	——	(0.027)	(0.002)	(0.001)
AL ($\alpha = 8$ deg)	Prediction	0.001	*−0.654*	*−0.043*	0.191	−0.000	*−0.181*	−0.269	0.074	−0.142	0.064	−0.001	*−0.048*	0.121	−0.436	0.044	−0.108
	(Variation)	(±0.006)	(±0.111)	(±0.010)	(±0.063)	(±0.004)	(±0.034)	——	——	(±0.022)	(±0.017)	(±0.001)	(±0.023)	——	——	(±0.014)	(±0.024)
	AL identification	0.001	*−0.883*	*−0.173*	0.227	0.000	*−0.115*	−0.190	[0.074]	−0.133	0.055	−0.001	*−0.020*	[0.121]	−0.226	0.038	−0.106
	(3σ)	(0.000)	(0.027)	(0.020)	(0.010)	(0.000)	(0.004)	(0.014)	——	(0.003)	(0.001)	(0.000)	(0.005)	——	(0.050)	(0.003)	(0.002)

[a]Aerodynamic model structure: $C_Y = C_{Y_0} + (C_{Y_\beta})\beta + (C_{Y_{\delta a}})\delta a + (C_{Y_{\delta r}})\delta r$, $C_l = C_{l_0} + (C_{l_\beta})\beta + (C_{l_p})\hat{p} + (C_{l_r})\hat{r} + (C_{l_{\delta a}})\delta a + (C_{l_{\delta r}})\delta r$, $C_n = C_{n_0} + (C_{n_\beta})\beta + (C_{n_p})\hat{p} + (C_{n_r})\hat{r} + (C_{n_{\delta a}})\delta a + (C_{n_{\delta r}})\delta r$.

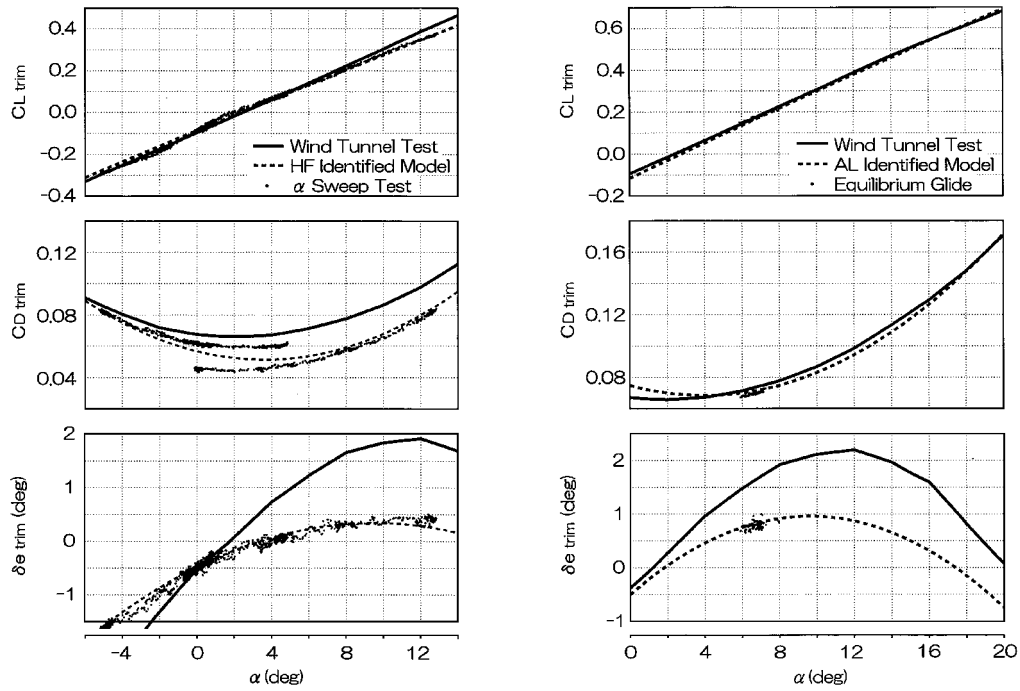

a) Hanging flight b) Automatic landing flight

Fig. 9 Longitudinal trimmed characteristics.

the vehicle during HF is estimated by subtraction of the tension of the hanging wire from the total external force, the load cell and the gimbal angles necessary to calculate the tension were subjected to sensitivity analysis. The locations of the load cell and the gimbals and the definition of the gimbal angles are shown in Figs. 10 and 11. The analysis clearly showed that a bias error of the gimbal pitch angle has the largest effect on the estimation error of the drag coefficient. To confirm this, the trimmed gimbal pitch angle in all the HFs was investigated, and it was found that the average value of the angle at each flight varied between approximately 3.5 and 5.0 deg. A bias error of 1.5 deg on the gimbal pitch angle results in an error of 0.02 for the drag estimation, consistent with Fig. 9, but results in an error of only 0.0002 for the lift estimation and has virtually no effect on the pitching moment characteristics (trimmed elevator angle) because the gimbal is set near the CG position. Judging from these analysis, the cause of the scattering of the trimmed drag coefficient estimated by the α sweep tests seems to be the measurement error of the gimbal pitch angle. One possible cause of the scatter of the gimbal pitch angle between trials is the umbilical cable fixed to the hanging wire, as shown in Fig. 10. The umbilical cable is used to supply electrical power and to send command signals to the vehicle during hanging flight, and it is thought that the direction of the gimbal might not have been coincident with the axis of the load cell because of the influence of this cable. If the umbilical cable were removed or made thinner by use of an internal battery to supply the vehicle's electrical power in HF, the cause problem would be eliminated. The drag characteristics extracted from the AL-identified model coincide with those extracted from equilibrium glide data of the five flights, and there is no discordance that was seen in the HF-identified model. The results of the AL flights seem to be reliable because the test data are not subject to measurement errors in the tension of the hanging wire. The fact that scattering of the flight test data (dashed–dotted curves) for the AL-identified model in Fig. 8 is much smaller than that of the flight test data for the HF-identified model indicates that the AL flight test data are less affected by measurement errors than HF test data. It was also clarified by the sensitivity analysis that the error of gimbal roll angle has a large effect on the estimation error of the side-force coefficient and the error of the load cell affects the lift coefficient. It should be noted that the estimation of the lift coefficient is affected very much by the measurement accuracy of the load cell, but the effect seems to be very small in this case because the estimated results by the HFs and AL flights for the lift coefficient coincide with each other very well. The pitching moment characteristics obtained from the HFs and AL flights are similar to each other and the results seem to be reliable. They are, however, different from those of the wind-tunnel model, and, furthermore, longitudinal static instability estimated from flight tests is smaller than the prediction of the wind-tunnel model for most of the angle of attack range (α less than 12 deg). If the estimated results extracted from the flight tests do have errors, one possible source is in the error of the estimated position of the vehicle's CG, which was estimated experimentally. In the case in which the CG position estimate used in the flight test data analysis is on the more unstable side (aft) of its actual position, this discrepancy will be reflected in the analysis results. The difference between actual and estimated CG positions that would result in the observed discrepancy between flight-test- and wind-tunnel-derived pitching moment characteristics has been calculated to be 30 mm. Judging from the fact that the experiment to estimate CG position should not have this large of an error and from the fact that the flight test results agree with the results of the hanging wind-tunnel tests[3] (conducted at the large-scale low-speed wind tunnel, NAL, in 1995, in which the HF was simulated inside the wind tunnel), it may be concluded that the wind-tunnel database for pitching moment has some error that is due to, for example, the sting effect.

Results of Estimation of Lateral-Directional Aerodynamic Characteristics

Table 2 shows the analytic model structures used for lateral-directional aerodynamic model identification from the dynamic flight test data and estimated model parameters of the HF- and the AL-identified models with the predicted parameters. As the lateral-directional characteristics change greatly with angle of attack, the predicted parameters to be compared with the results of the HFs are calculated with the wind-tunnel model at $\alpha = 0$ deg because the control system was used to maintain the angle of attack at 0 deg during the flight tests for the estimation of the lateral-directional characteristics. On the other hand, those for the AL flights are calculated with the wind-tunnel model at $\alpha = 8$ deg because the vehicle

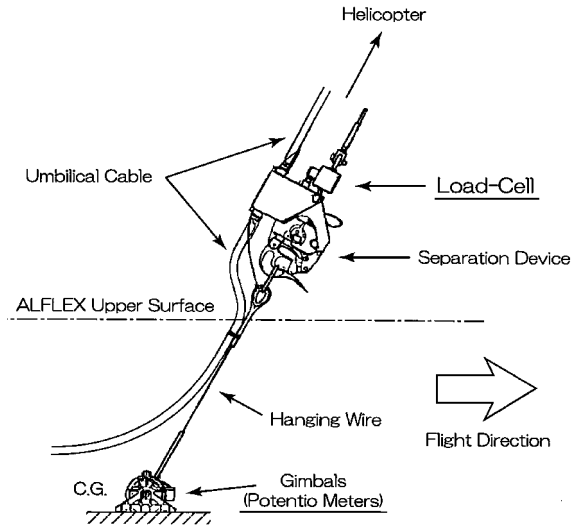

Fig. 10 Schematic of hanging system.

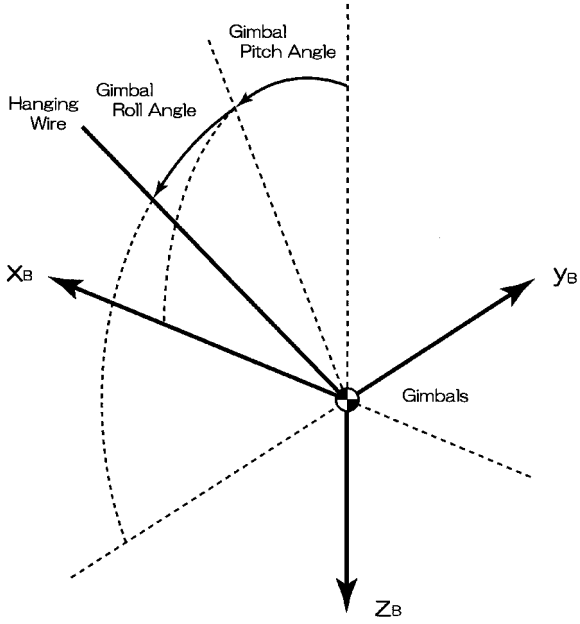

Fig. 11 Definition of gimbal pitch/roll angle.

flies near this angle of attack during the equilibrium glide phase at which the dynamic tests were performed. As a result, the predicted parameter values for HFs and AL flights are different. For dynamic parameters, only the roll damping C_{l_p} and the yaw damping C_{n_r} are estimated, fixing the cross terms C_{l_r} and C_{n_p} at the predicted values, because it is difficult to separate roll and yaw motions. Judging from Table 2, all the estimated parameters relating to the side-force coefficient of the HF-identified model are outside the variation except for the effect of the rudder ($C_{Y_{\delta r}}$). In particular, the difference of the constant term C_{Y_0} comes up to 200% of the variation. The most possible cause for this difference is the measurement error of the gimbal roll angle, as stated in the preceding section. Other possible causes are asymmetry of the aerodynamic characteristics and biases in the measurements of δa, δr, β, and a_y side acceleration. The difference of side-force slope C_{Y_β} is ~120% of the variation. It might also be affected by scattering in gimbal roll angle between trials. For the rolling and yawing moment coefficients, all the estimated parameters of the HF-identified model are within the variations. Both the estimated roll damping C_{l_p} and the yaw damping C_{n_r} are approximately 75% of their predicted values. The aileron and rudder effects ($C_{l_{\delta a}}$, $C_{n_{\delta a}}$, $C_{l_{\delta r}}$, and $C_{n_{\delta r}}$) are estimated at 83–105% of their wind-tunnel prediction values. For the AL-identified model, there is little bias of the side-force coefficient, which was observed in the HF-identified model. The differences between the other parameters of the AL-identified model and the predicted model are similar to those between the HF-identified model and its corresponding predicted model except for the β derivatives, but the differences in β derivatives of all three coefficients (C_{Y_β}, C_{l_β}, and C_{n_β}) are outside the variations. This is due to the fact that variation of the sideslip angle during the maneuver was small compared with measurement noise. The effects of the control surfaces are estimated at 86–98 % of values predicted from wind-tunnel data.

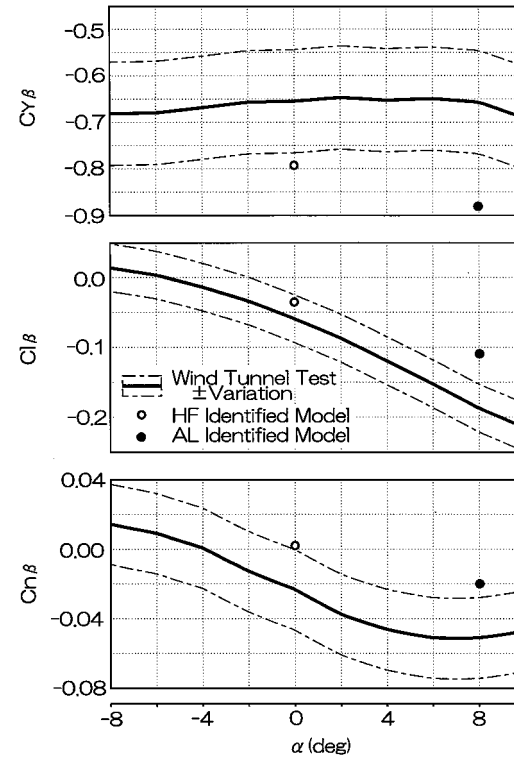

Fig. 12 Lateral-directional identified model.

The graphs in Fig. 12 show the relationship between the β derivatives of the HF- and the AL-identified models and the wind-tunnel model, with α as the abscissa parameter. In these figures, the dashed–dotted curves indicate the variations of the wind-tunnel model.

Figure 13 shows the lateral-directional trimmed characteristics extracted from the quasi-steady flights (β sweep and the equilibrium glide) and those calculated with the three aerodynamic models (the HF- and the AL-identified models and the wind-tunnel model). For HF, the trimmed aileron angle (δa_{trim}) and the trimmed rudder angle (δr_{trim}) calculated with the HF-identified model and the results of the β sweep test agree well and these results also appear reliable, taking into account the fact that the identified model parameters are within the variations. For the trimmed side-force coefficient $C_{Y_{\text{trim}}}$, although the HF-identified model parameter's slope vs sideslip angle coincides with the values derived from the β sweep test, there is a large bias. This might occur because the gimbal roll angle varies between the dynamic flight tests and the β sweep tests, similar to the gimbal pitch angle in the estimation of the drag coefficient. Examining the results of the automatic landing flight, we see that there is no discrepancy between the AL-identified model, wind-tunnel model, and the equilibrium glide data, and no aerodynamic asymmetry is apparent. As was stated before, the lateral-directional characteristics change greatly with angle of attack and since the HF and the AL flight tests for aerodynamic characteristic estimation were conducted at different angles of attack, the estimated HF and AL flight lateral-directional characteristics cannot be compared.

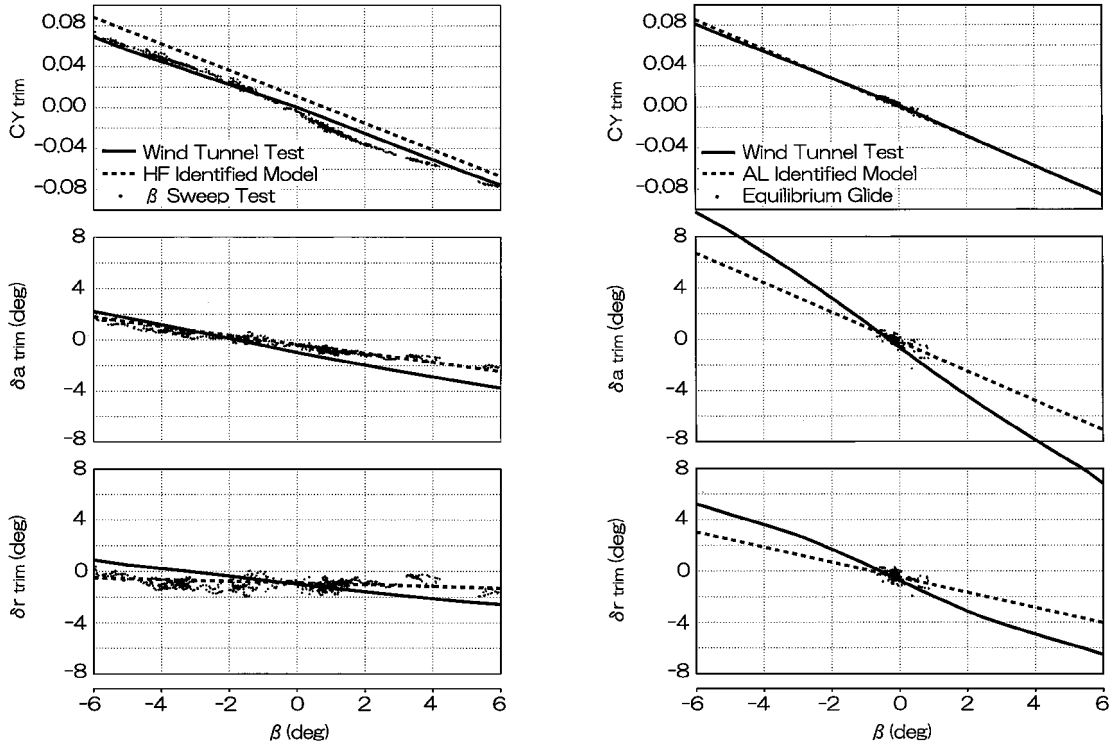

a) Hanging flight, α = 0 (deg) b) Automatic landing flight, α = +8 (deg)

Fig. 13 Lateral-directional trimmed characteristics.

Summary of Results

Lift Coefficient

All the estimated values of the constant term C_{L_0} and the lift curve slope C_{L_α} compare well with the wind-tunnel predictions. The elevator and the speed-brake effects are so small that estimation through flight testing was difficult.

Drag Coefficient

In the results obtained from the HFs there are biases that are different from each flight and seem to be caused by the measurement error of the gimbal pitch angle. However, the results of the AL flights, which are free of the gimbal angle problem, compare well with the wind-tunnel data and seem to be reliable. Although the effect of the speed-brake ($C_{D_{\delta s}}$) is estimated from only the AL flights, it compares well with the wind-tunnel data.

Pitching Moment Coefficient

The pitching moment characteristics obtained from HF and AL flight tests are similar to each other, but both differ from wind-tunnel measurements, although the differences are within the variations. A possible cause of these differences is measurement error in the wind-tunnel data that is due to the effect of a supporting device. The pitch damping parameters C_{m_q} and the elevator effects $C_{m_{\delta e}}$ estimated from the HFs and the AL flights are very close to the wind-tunnel predictions.

Side-Force Coefficient

In HF test results, there is a bias error that is possibly caused by measurement error of the gimbal roll angle. That is not seen in the AL flight test results, but the error of β derivative C_{Y_β} estimated by the AL flights is larger than that in the HF. The reason for this is that the variation of the sideslip angle during the maneuver was small compared with measurement error. Both of the rudder derivatives $C_{Y_{\delta r}}$ estimated from the HF and the AL flight are within the variations.

Rolling Moment Coefficient

All parameters estimated by the flight tests, except for the β derivative C_{l_β} derived from the AL flight test results are within the variation.

Yawing Moment Coefficient

There is a large difference between the β derivative C_{n_β} estimated by the AL flights and the wind-tunnel database, as with other lateral-directional coefficients. Other estimated parameters compare well with the wind-tunnel predictions.

Conclusions

The aerodynamic characteristics of the ALFLEX vehicle were estimated by HF and AL flight tests. Most of the results compared well with wind-tunnel predictions. The pitching moment characteristics estimated from the flight tests differed from wind-tunnel measurements, but the differences were within the variation. In the HFs, the estimated results for the drag coefficient and the side-force coefficient were scattered because of measurement errors of the gimbal angles caused by the effects of the umbilical cable connecting the ALFLEX vehicle and the mother helicopter. The characteristics except for the above are estimated well by the HFs, and the method was shown to be useful. More accurate estimation will be possible if the effect of the umbilical cable can be reduced, for example, by use of an internal battery to supply electrical power to the vehicle during hanging flight.

References

[1] Davis, N. W., "NASDA Pins Its Hopes on HOPE," *Aerospace America*, Vol. 29, No. 8, 1991, pp. 32–35.

[2] Tsukamoto, T., Yanagihara, M., Nagayasu, M., and Sagisaka, M., "ALFLEX Five Degrees of Freedom Hanging Flight Test," AIAA Paper 97-3484, Aug. 1997.

[3] Yanagihara, M., "Suspending Wind-Tunnel Test for ALFLEX Vehicle," National Aerospace Lab., Tokyo, TR-1306, Sept. 1996 (in Japanese).